# Lagrangian Coherent Structures as a new frame to investigate the particle transport in highly chaotic magnetic systems

IOP Conf. Series: Journal of Physics: Conf. Series **1125** (2018) 012008 doi:10.1088/1742-6596/1125/1/012008

# Lagrangian Coherent Structures as a new frame to investigate the particle transport in highly chaotic magnetic systems

**G. Di Giannatale[1], M.V. Falessi[2],D. Grasso[3], F. Pegoraro[4], T.J. Schep[5], M. Veranda[1], D. Bonfiglio [1], S. Cappello[1]**

[1] Consorzio RFX (CNR, ENEA, INFN, Università di Padova, Acciaierie Venete SpA) Corso Stati Uniti 4, Padova, Italy
[2] ENEA, C. R. Frascati, Via E. Fermi 45, Frascati, Italy
[3] ISC - CNR and Politecnico di Torino, Dip. Energia C.so Duca degli Abruzzi 24, Torino. Italy
[4] Dip. Fisica E. Fermi, Pisa University, largo Pontecorvo 3, Pisa, Italy
[5] Dep. Applied Physics, Eindhoven Univ. of Technology, 5600MB Eindhoven, The Netherlands

E-mail: giovanni.digiannatale@igi.cnr.it

**Abstract.** The concept of Lagrangian Coherent Structures (LCS) is here applied to investigate in a new perspective the particles transport in chaotic magnetic configurations. A paradigmatic and simplified magnetic configuration is revisited before extending the analysis to a more realistic one. Preliminary results concerning the typical dynamics of the Reversed Field Pinch (RFP) device are shown.

## 1. Introduction

The transport of particles along chaotic trajectories is an important issue in thermonuclear plasmas, since magnetic field lines embedded in a plasma confinement system are often characterized by a chaotic motion [1, 2, 3, 4, 5, 6]. Even though this circumstance may lead to a degradation of the confinement properties, also in a chaotic domain magnetic barriers can emerge and limit the field line motion itself. In this work we still remain within the ansatz of the motion of magnetic field line as a proxy for the particle trajectories along the lines. This has been a common ansatz in fusion plasmas where collisions effects and drifts are neglected (see for example the famous paper [7]) and it proved to be valid when using test electrons to reconstruct the magnetic topology of Wendelstein 7-X [8] .
In this frame, the possibility of distinguishing in a chaotic domain sub-regions having different transport behaviour becomes crucial. Several types of techniques, such as orbit stickiness, finite time rotation number, and braiding exponents, have also been used in the literature in order to partition the regions with different dynamical properties in Hamiltonian systems,see e.g. [9, 10, 11, 12].

In this work we apply the concept of Lagrangian Coherent Structures (LCSs) borrowed from the study of dynamical systems [see the review paper in [13]] in order to distinguish in a chaotic domain sub-regions characterized by different transport features. The LCS concept has been introduced in Ref. [14] in order to generalize the dynamical structures observed in autonomous

and periodic systems to temporally aperiodic flows. In this perspective over the finite time span which characterizes the LCS the particles belonging to different regions can not mix with each other.
In plasmas environment these studies have been carried out, e.g. [15],[16], studying transport barriers for a fixed dynamical time. Here we review the works [17, 18], where we have applied the concept of Lagrangian Coherent Structures (LCSs) to a paradigmatic chaotic magnetic field configuration, generated by a magnetic reconnection event, in order to separate regions where field lines have a different kind of behaviour. In addition we have considered the possibility that the magnetic field evolves in time during the particle transit time. To take into account the dynamical time dependence we define LCS that depend on the particle velocities. In this way we are able to test if particles with different energies experience different transport barriers. In addition to this review, following previous work [16], we apply the adopted definition of LCS to a more realistic situation.

We will consider the numerical simulations of a Reveresed-Field-Pinch configuration, characterized by a broad chaotic region and will investigate the presence of transport barriers. At this stage the analysis will be restricted to the time-periodic case.

## 2. Lagrangian Coherent Structures as maximal repulsion-attraction material lines

We consider a dynamical system in 2D phase space $\boldsymbol{x} = (x, y)$ with continuous differentiable flow map

$$\boldsymbol{\phi}_{t_0}^{t}(\boldsymbol{x}_0) = \boldsymbol{x}(t, t_0, \boldsymbol{x}_0). \tag{1}$$

Two neighbouring points $\boldsymbol{x}_0$ and $\boldsymbol{x}_0 + \boldsymbol{\delta} x_0$ evolve into $\boldsymbol{x}$ and $\boldsymbol{x} + \boldsymbol{\delta} x$ according to

$$\boldsymbol{\delta} x = \boldsymbol{\nabla} \boldsymbol{\phi}_{t_0}^{t}\, \boldsymbol{\delta} x_0. \tag{2}$$

Consider a curve $\gamma_0$ and at each point $\boldsymbol{x}_0 \in \gamma_0$ define the unit tangent and normal vectors $\boldsymbol{e}_0$ and $\boldsymbol{n}_0$. In the interval $[t_0, t]$, $\gamma_0$ evolves into $\gamma_t$, and $\boldsymbol{x}_0 \in \gamma_0$ into $\boldsymbol{x}_t \in \gamma_t$. The tangent vector $\boldsymbol{e}_0$ evolves, by means of the linearized dynamics, into

$$\boldsymbol{e}_t = \frac{\boldsymbol{\nabla} \boldsymbol{\phi}_{t_0}^{t}(\boldsymbol{x}_0)\, \boldsymbol{e}_0}{[\boldsymbol{e}_0\, \boldsymbol{C}_{t_0}^{t}(\boldsymbol{x}_0)\, \boldsymbol{e}_0]^{1/2}}, \tag{3}$$

and the normal vector $\boldsymbol{n}_0$ into

$$\boldsymbol{n}_t = \frac{\left(\boldsymbol{\nabla} \boldsymbol{\phi}_{t}^{t_0}\right)^T \boldsymbol{n}_0}{[\boldsymbol{n}_0\, \boldsymbol{C}^{-1}(\boldsymbol{x}_0)\, \boldsymbol{n}_0]^{1/2}} \tag{4}$$

where $^T$ stands for transposed and $\boldsymbol{C}_{t_0}^{t}(\boldsymbol{x}_0) \equiv \left(\boldsymbol{\nabla} \boldsymbol{\phi}_{t_0}^{t}\right)^T \boldsymbol{\nabla} \boldsymbol{\phi}_{t_0}^{t}$ is the *Cauchy-Green strain tensor* which describes the deformation into an ellipse of an arbitrarily small circle of initial conditions (i.c.), centered in $\boldsymbol{x}_0$ and $\boldsymbol{C}^{-1}(\boldsymbol{x}_0) = \boldsymbol{C}_{t}^{t_0}(\boldsymbol{x}_0)$. To simplify the notation the time interval marks have been suppressed as will be the case in the following formulae. Let $\boldsymbol{\xi}_{max}$ and $\boldsymbol{\xi}_{min}$ be its two eigenvectors with positive eigenvalues $\lambda_{max}$ and $\lambda_{min}$. The curves with tangent vector along $\boldsymbol{\xi}_{min}$ and, respectively, $\boldsymbol{\xi}_{max}$ are called *strain lines* of the Cauchy-Green tensor. The *repulsion ratio* $\rho_{t_0}^{t}(\boldsymbol{x}_0, \boldsymbol{n}_0)$ is defined (see Ref.[19, 20]) as the ratio at which points initially near $\boldsymbol{x}_0 \in \gamma_0$ increase their distance from the curve $[t_o, t]$:

$$\rho_{t_0}^{t}(\boldsymbol{x}_0, \boldsymbol{n}_0) = \boldsymbol{n}_t\, \boldsymbol{\nabla} \boldsymbol{\phi}_{t_0}^{t}(\boldsymbol{x}_0)\, \boldsymbol{n}_0 = [\boldsymbol{n}_0\, \boldsymbol{C}^{-1}(\boldsymbol{x}_0)\, \boldsymbol{n}_0]^{-1/2} = [\boldsymbol{n}_t\, \boldsymbol{C}(\boldsymbol{x}_0)\, \boldsymbol{n}_t]^{1/2}. \tag{5}$$

An LCS over a finite time interval $[t_0, t_0 + T]$ is defined as a material line along which the repulsion rate is pointwise maximal. This leads, as shown in Refs. [19, 20], to the following

definitions of Weak Lagrangian Coherent Structures and LCS.
A material line satisfying the following conditions at each point:

$$a) \qquad \lambda_{min} < \lambda_{max}, \quad \lambda_{max} > 1, \tag{6}$$

$$b) \qquad \boldsymbol{e}_0 = \boldsymbol{\xi}_{min} \tag{7}$$

the tangent vector is along the eigenvector associated with the smallest eigenvalue,

$$c) \qquad \boldsymbol{\xi}_{max} \cdot \boldsymbol{\nabla} \lambda_{max} = 0 \tag{8}$$

the gradient of the largest eigenvalue is along the curve, is called a repulsive Weak Lagrangian Coherent Structure (WLCS). A WLCS which satisfies at each point the additional condition

$$\boldsymbol{\xi}_{max} \cdot \boldsymbol{\nabla}^2 \lambda_{max} \cdot \boldsymbol{\xi}_{max} < 0 \tag{9}$$

is called a repulsive Lagrangian coherent structure. Attractive LCS are defined as repulsive LCS of the backward time dynamics. For a Hamiltonian flow (that is the case considered here) the flow map is incompressible (volume-preserving).

## 3. Slab magnetic field configuration

The magnetic field and the choice of time instants which we consider in this section have been obtained and discussed in Ref.[21], where the two-fluid equations have been solved for the magnetic flux and the stream function in slab geometry with periodic boundary conditions in all three directions. The magnetic equilibrium configuration is tearing unstable to the adopted multiple helicity initial condition. In this way a magnetic reconnection process with multiple island chains has been induced. The magnetic field is expressed in terms of the flux function $\psi$ as:

$$\mathbf{B} = B_0 \mathbf{e}_z + \nabla \psi(x, y, z, t) \times \mathbf{e}_z,$$

with $\psi(x, y, z, t) = 0.19 \cos(x) + \hat{\psi}_1(x, t) \cos(k_{1y} y + k_{1z} z) + \hat{\psi}_2(x, t) \cos(k_{2y} y + k_{2z} z)$ in the domain $[-L_x, L_x] \times [-L_y, L_y] \times [-L_z, L_z]$ with $L_x = \pi$, $L_y = 2\pi$, $L_z = 16\pi$ with $k_{1y} = k_{2y} = 2\pi/L_y$ and $k_{1z} = 0$ while $k_{2z} = 2\pi/L_z$. The initial perturbations, $\hat{\psi}_1(x, 0)$ and $\hat{\psi}_2(x, 0)$, are localized at the resonant surfaces $x_1 = 0$ and $x_2 = 0.71$ respectively. At each fixed physical time $t$ the magnetic flux function $\psi(x, y, z, t)$ plays the role of the Hamiltonian for the magnetic field lines with $x$ and $y$ canonical variables and $z$ the magnetic Hamiltonian time ($t_H$). The field line equations become $dx/dz = -\partial\psi/\partial y$ and $dy/dz = \partial\psi/\partial x$. The presence of a double helicity perturbation guarantees the non-integrability of the system and the generation of a chaotic behaviour of the magnetic field lines. In particular, as described in detail in Ref.[21], the process develops following three phases. A linear one in which two independent island chains are formed at their resonant surfaces. A quasi-linear phase in which the island chains grow to such an extension that they start to interact inducing a chaotic behaviour of magnetic field lines. Chaos develops around the separatrix of the magnetic islands firstly and then it spreads all around as reconnection evolves in the last non linear phase.

We will consider the normalized physical time ($t_P$) interval $t = 415 - 425$ in which chaos, initially developed only on a local scale (at $t = 415$), starts to spread on a global scale (at $t = 425$).

First we consider the dynamical system obtained by taking a snapshot at a given $t_P$ where the flux function $\psi(x, y, z, t = \bar{t})$ is the Hamiltonian and $z$ is the $t_H$. The periodicity in the $z$-direction allows us to exploit the Poincaré map technique, which gives a detailed picture of the chaotic domains, provided one integrates the Hamilton equations starting from a sufficiently large number of initial conditions and for sufficiently large values of the $t_H$ parameter. These

results will be compared with the LCS approach. The attractive LCS will be found as mirror images of the repulsive ones with respect to $y = 0$, due to the symmetry property $\psi(x, y, z, t = \bar{t}) = \psi(x, -y, -z, t = \bar{t})$.
Subsequently,the particle motion in a time-varying magnetic field will be considered through a simplified model. In this model particle gyromotion and drifts are neglected and the particle dynamics is retained only through their (constant) streaming velocity $V$ along the guide field $B_0$. Adopting this point of view we are able to describe the LCSs in a time nonperiodic dynamical system and to identify LCSs that depend explicitly on the different particle velocities. Thus we introduce a family of nonautonomous dynamical systems characterized by a different velocity $V$, with Hamiltonian $\psi_{\mathcal{V}}(x, y, z) \equiv \psi(x, y, z, t = t_0 + (z - z_o)/V)$. In the following we assume $V > 0$. For negative $V$ and for the modified relationship between repulsive and attractive LCSs see Ref.[17]. The velocity is normalized to the Alfvèn velocity (coherently with the normalization of the time-scale) based on the characteristic magnitude of the equilibrium magnetic field in the plane perpendicular to the z-direction, $B_{y0}$. The chosen values for the velocity are a compromise between having a magnetic field that does not evolve too fast during the motion of particles and being able to show the dependence of the LCS on the velocity V and to investigate whether or not the LCS computed for a given velocity $V$ act as barrier also for particles with different velocities.In order to make this condition quantitative, we observe that we cannot apply straightforwardly the standard definition based on the ratio between the particle transit time through the configuration and the magnetic field growth time because in the physical time interval $t = 415, 425$ the evolution of the magnetic field is super-exponential [21]. However we can provide an estimate by considering the ratio $R$ between the number of loops that a particle moving with velocities $V_{1,2}$ makes during this interval and the factor by which the main $(1, 0)$ mode has grown in the same interval. For $V_1 = 1000$ we find $R = 88$ while for $V_2 = 200$ we find $R = 17.6$ which show that even the slower particles make in the interval $t = 415, 425$ a number of loops that is sufficient to experience the effect of the LCS.

## 4. Numerical results

To find the hyperbolic LCSs we used the MATLAB tool developed by Onu et al. in Ref. [22]. This tool is based on the identification of the LCS as the most repelling curves. These curves are identified as those passing through a local maximum of the Finite Time Lyapunov Exponet (FTLE) field related to the Cauchy-Green strain tensor field, defined in the previous section. Since in chaotic systems, the FTLE field exhibits an exceedingly large number of local maxima, by integrating the above condition for each of them, we would find so many structures that no physical information could be extracted. For this reason we have introduced a criterion to select the most relevant LCS. The details of the application and optimization of this procedure are available in Ref.[18].

### *4.1. $t_H$ periodic results*

The investigation of transport barriers has been initially done in the $t_H$ periodic case. In this frame we study the transport barrier at fixed physical time. In practical sense, these are transport barriers for particles having a very short z-transit time along the periodic direction with respect to the time-scale variation of the magnetic field. In the left panel of Fig. 1 we show the agreement between the Poincaré map and the LCS (attracting in blu and repelling in red). The green arrows highlight the intersection between the attracting and the repelling LCS. This behaviour is not surprising, because LCSs generalize what stable and unstable manifolds are for a Hamiltonian system. We refer to the Ref. [17] for the analogy between the LCS and Hamiltonian structure of a non-integrable system. This figure shows only few LCS (the ones we consider the strongest) but additional LCS can be found relaxing some numerical parameters (see Ref. [18]). In the right panel of Fig. 1 we check if the LCS we have found act as transport barriers. To this aim

we put several initial conditions in a very narrow region (denoted by the green arrow) and then we evolve these initial conditions under the flow by integrating the magnetic field line equations until they perform 150 z-loops. In principle, to check if an LCS does confine the particles, one should evolve under the flow map $\Phi$ both particles and the LCS itself, checking that at each time step particles do not cross the LCS. But, due to the nature of the dynamical system we are considering (chaos not totally developed), the LCS we found mark invariant manifold or regular surviving tori making the LCS invariant under the flow map. Of course, when the system loses its periodicity this argument does not hold anymore.

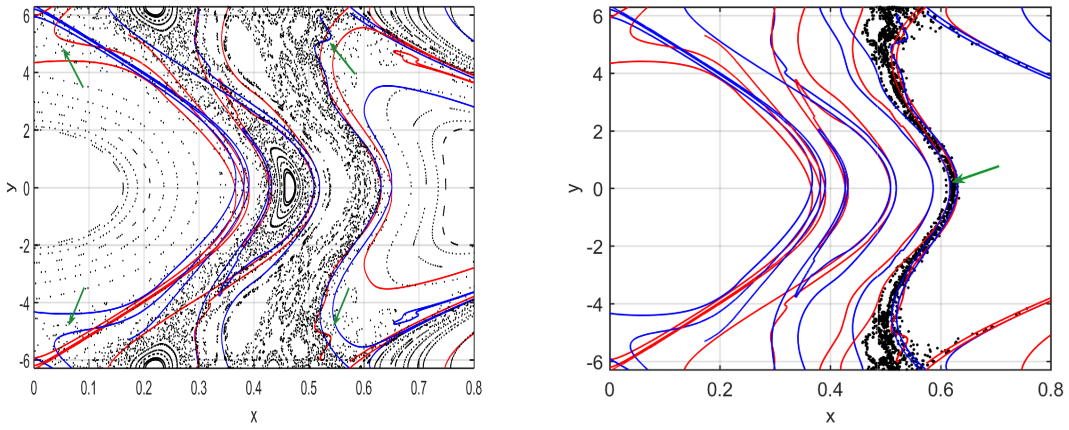


**Figure 1.** In the left panel the most important LCS are overplotted on the Poincaré map at $z = 0$ and $t = 415$. The repelling (attractive) structures are drawn in red (blue). In the right panel it is shown that i.c. located where the green arrow points cannot cross the barrier.
Reproduced from Ref. [18], with the permission of AIP Publishing

*4.2. $t_H$ non periodic results*

In the case of $t_H$ non periodic, it is not possible to check the agreement between the LCS and the Poincaré map. Indeed, even if we follow the magnetic field lines and plot them each time they go through a plane z-costant (puncture plot), the resulting plot would give only information about the mean value of the radial transport, but it would not allow to extract information about a partition of the space (thus transport barriers cannot be seen). This is due to the fact that islands are moving because the perturbation grows in time. Then the resulting puncture plot would result in a mix of dots without any kind of topological information.

Thus, to check the validity of LCS we need to follow in time (and space) both LCS and particles. We remember that time and space are related, so the Hamiltonian is $\psi_{\mathcal{V}}(x, y, z) \equiv \psi(x, y, z, t = t_0 + (z - z_o)/V)$. where $t_0 = 415$. In Fig. 2 is shown the position at $t = 415.1$ and $t = 417$, in the left and right panel respectively, of two sets of i.c. initially separated by a LCS. In the first part of the dynamics, particles tend to go as far as possible from the repelling LCS. Of course this motion happens in the perpendicular direction, coherently with the fact that the particles maximize their distance from the LCS.

In the right panel, it is clear that each set of particles obeys to its own dynamics. The black i.c. stretched increasing their mixing, while the green i.c. remained compact. This is due do the fact that the black i.c. have been located over an attracting LCS (let us image this i.c. as a blob of fluid crossed by an attracting LCS), whereas the green i.c. have been located in a region without attracting LCS.

Moreover, since we take into account the time evolution of the field by a relation between the z-position and the velocity, it is clear that now the Hamiltonian depends on the particle velocity. This relation gives rise to the possibility that particles having different velocities may see different transport barriers.

In Fig. 3 the attracting LCS computed for particles having $V = 1000$ are shown in both panels. In the left (right) panel the positions of several sets of particles, initially located in different positions of the domain and having $V = 1000$ ($V = 200$ ) are overplotted. We observe that, although the particle positions for $V = 200$ appear qualitatively similar to those in left panel, they are shifted towards higher $x$-values with respect to black particles having $V = 1000$, and thus there is no agreement between the LCS, that have been computed for particles having $V = 1000$, and the particles position. This can be understood, since the particles having $V = 200$ see a stronger chaos (with respect to particles with $V = 1000$) that decreases the area of the $m = 2$ island chain.

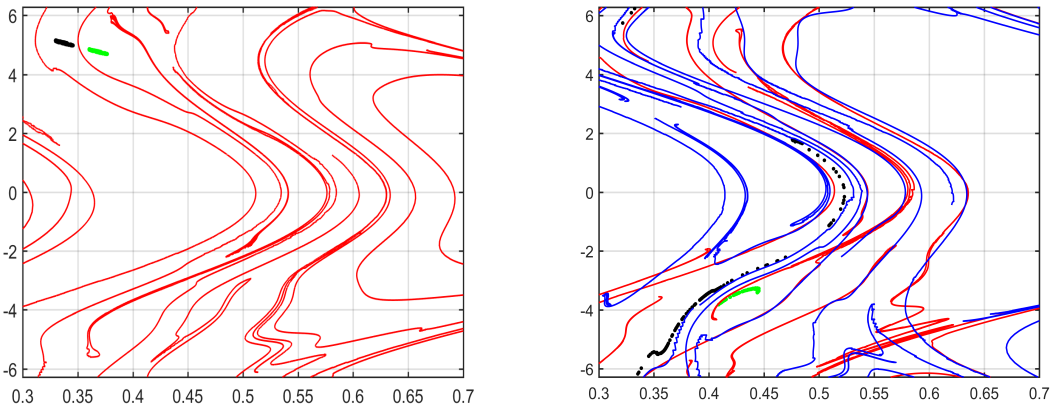


**Figure 2.** Position of i.c. separated by a LCS at $t = 415.1$ (417) on the left (right) panel. Reproduced from Ref. [18], with the permission of AIP Publishing

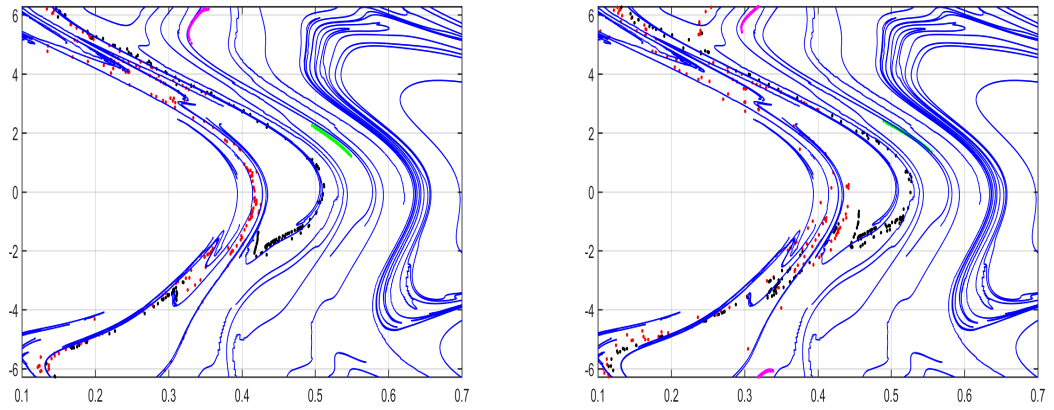


**Figure 3.** In both panels the LCS evaluated for $V = 1000$ are plotted. In the left (right) panel the location of evolution of different sets of i.c. evaluated for $V = 1000$ ($V = 200$). Reproduced from Ref. [18], with the permission of AIP Publishing

## 5. Reversed Field Pinch numerical simulation

A numerical simulation of the reversed-field pinch (RFP) configuration for the magnetic confinement of fusion plasmas has been performed using the spectral code Specyl ( Ref. [23]). Specyl solves the visco-resistivity MHD equations with the zero pressure and constant density ($\rho = 1$ in the momentum equation) approximation. The equations written in dimensionless units are:

$$\partial_t \mathbf{v} + \mathbf{v} \cdot \nabla \mathbf{v} = \mathbf{J} \times \mathbf{B} + \nu \nabla^2 \mathbf{v} \quad (10)$$

$$\partial_t \mathbf{B} = \nabla \times (\mathbf{v} \times \mathbf{B} - \eta \mathbf{J}) \quad (11)$$

$$\nabla \times \mathbf{B} = \mathbf{J} \quad (12)$$

$$\nabla \cdot \mathbf{B} = 0 \quad (13)$$

Numerical simulations are performed in cylindrical geometry with aspect ratio $R_0/a = 4$, where $a = 1$ is the cylinder radius and $2\pi R_0$ the periodicity of the cylinder in the axial direction.

The simulation takes into account a nonuniform resistivity, $\eta = \eta_0(1 + 20(r/a)^{10})$ with $\eta_0 = 10^{-6}$ and an uniform viscosity $\nu = 10^{-4}$. The magnetic boundary conditions are helically modulated by imposing a Magnetic Perturbation (MP) having a poloidal periodicity $m = 1$ and cylindrical periodicity $n = 6$ (thus, for the chosen parameters of simulation, a non resonant MP), see further details in Ref. [24].

The RFP dynamics was characterized by a strong activity of several MHD modes, whose interaction tended to generate a stochastic magnetic field. In the late '90 it was discovered the possibility of cycles of Quasi-Single Helical (QSH) states formation, during which a single MHD mode was able to grow more intense than the other MHD modes, to give its own helicity to the core region of the plasma [25, 26], with beneficial effects on the magnetic field topology [25, 27, 28, 29]. In the new states such a topology consists of core-conserved and edge-conserved magnetic surfaces. The first belong to the set colored in green in the bottom panel of Fig. 4. In this figure we show the magnetic field topology during the dynamical phase, highlighted by the stripes in the top panel of Fig. 4, of quasi-periodical formation of QSH states. In this case, the helical winding of the plasma column is the same given to the plasma through the MP.

Here we are interested in evaluating if, in this phase of the simulation, some magnetic transport barriers exist. Applying the LCS technique, we find the barriers shown in black in the left panel of Fig. 5. Like in the results of the model described in Sec. 3, also for this more realistic and complex configuration the LCS technique allows a more refined analysis, highlighting some structures in region where the Poincaré map suggests only a stochastic behaviour. To check the robusteness of the barriers, we take two sets of initial conditions separated by an LCS and evolve these two sets under the flow map. The result is shown in the right panel of Fig. 5, where four different regions separated by LCS are clearly visible. Indeed, evolving the particles under the flow, not only the red i.c. and the blu i.c. stay apart, but a further partition of the space, underlined by the fact that red i.c. cannot access the region on their left and blue i.c. cannot access the region on their right, emerges. Thus we conclude that this structures act as transport barriers for a finite time. Such a time during which magnetic field lines are confined by a LCS, $\hat{t}$, is longer than the other relevant time scales in MHD and in experiment. In fact, a test particle in RFX-mod ($R_0 = 2$m) with a typical temperature of $T \sim 700$ eV and with the mass of an electron would cover the length $L = 100Lz \sim 1.2\ 10^3$m in a time scale $\hat{t} = L/v_{th} = L/\sqrt{(2T/m_e)}$ that is longer than the typical dynamical scales ($\hat{t}/\tau_A \sim 10^3$) and longer than the typical collisional time between electrons and ions ($\hat{t}/\tau_{ei} \sim 10$).

## 6. Conclusions and remarks

In this paper we have used the conceptual framework of the Lagrangian Coherent Structures to analyze two magnetic configurations characterized by a chaotic behavior of the field lines,

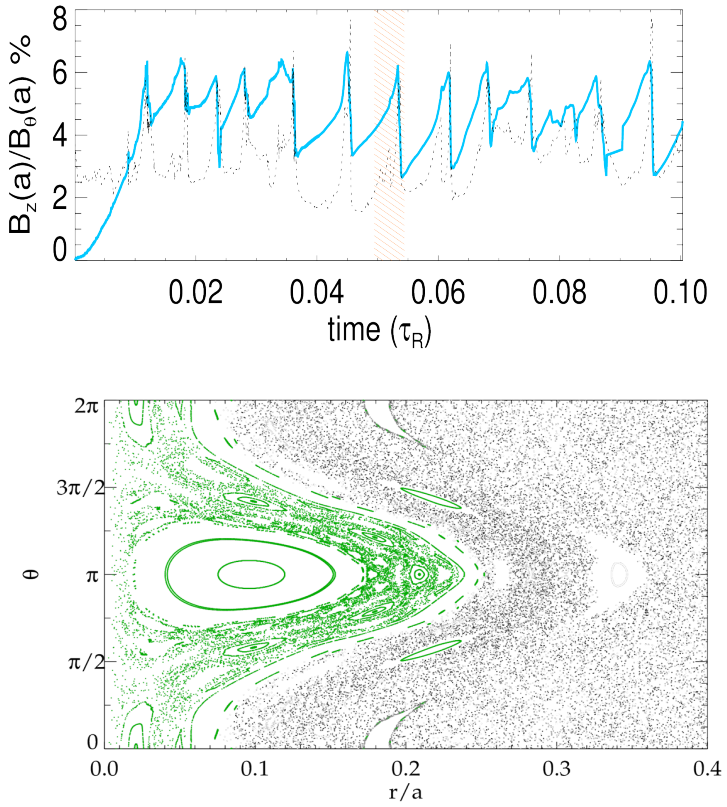


**Figure 4.** (Top) Dynamical behaviour of QSH MHD cycle in a RFP device. (Bottom) Poincaré map during the dynamical phase highlighted by the stripes in the top panel. Among the green dots, marking the magnetic field lines whose maximal radial position during their whole evolution is below $\hat{r} = 0.25a$, it is possible to recognize the core conserved region.

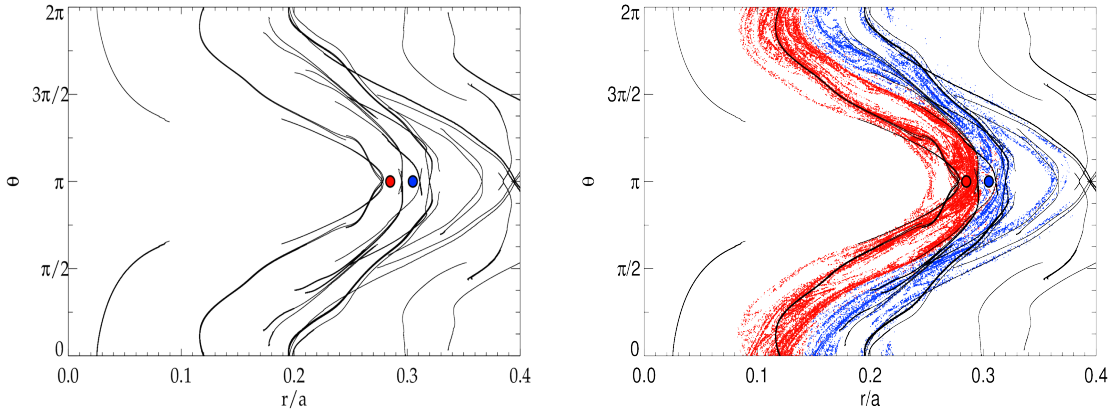


**Figure 5.** LCS and two set of initial condition (left pannel) and LCS with evolution of initial condition up to 100 z-loop (right pannel).

intended as a first approximation of the particle motion (particles moving along the field lines). The first configuration analyzed was derived by a numerical experiment of magnetic reconnection

and was meant to provide a study-case useful to illustrate the adopted technique. We have firstly revisited the case of a fixed dynamical time, corresponding to a particle motion with infinite velocity along the magnetic field lines. Secondly, we have introduced in an simplified way the dependence from the dynamical time of the process, showing that particles with different velocities experience different barriers. The second configuration analyzed was derived by numerical simulations of the RFP configuration reproducing the transition to the QSH state, and was meant to illustrate the use of the LCS in a more realistic configuration. In this case the LCS technique allowed to identify magnetic barriers in the chaotic area that were not detected by the inspection of the Poincaré maps only. In both analyses the LCS technique gives a complete partition of the space, showing that there are regions in which particles are embedded and in which mixing processes can develop on different time-scales. It has been also proved that these structures split a region in sub regions among which the transport is not allowed. We remark that the approach adopted above is limited to a test particle analysis which is not constrained to be consistent with the magnetic field via Ampere's Law. Finally we recall that the goal of this paper is to give a description of how to partition the chaotic domain of a 3D magnetic field. The same technique can be used, knowing the full Hamiltonian of a particle, to study the chaotic motion of particles that, as shown in [30], can appear also for magnetic configurations having a well preserved flux surfaces.

[1] Lorenzini R et al. 2009 *Nature Physics* **5** 570
[2] Firpo M C, Lifschitz A F, Ettoumi W, Farengo R, Ferrari H E and García-Martínez P L 2017 *Plasma Phys. Control. Fusion* **59** 034005
[3] Hatch D R, Pueschel M J, Jenko F, Nevins W M, Terry P W and Doerk H 2012 *Phys. Rev. Lett.* **108** 235002
[4] Nevins W M, Wang E and Candy J 2011 *Phys. Rev. Lett.* **106** 065003
[5] Suzuki Y et al 2012 *Proc. 24th IAEA Fusion Energy Conf. (San Diego, CA,) (Vienna: IAEA) EX/P8-1*
[6] Schmitz O et al. 2008 *Nuclear Fusion* **48** 024009
[7] Rechester A and Rosenbluth M 1978 *Phys. Rev. Lett.* **40** 38
[8] Sunn Pedersen T, Otte M, Lazerson S, Helander P, Bozhenkov S, Biedermann C, Klinger T, Wolf RC, Bosch HS and The Wendelstein 7-X Team 2016 *Nature Commun.* **7** 13493
[9] Hudson S R and Breslau J 2008 *Phys. Rev. Lett.* **100** 095001
[10] Misguich J H, Reuss J D, Constantinescu D, Steinbrecher G, Vlad M, Spineanu F, Weyssow B and Balescu R 2002 *Plasma Phys. Control. Fusion* **44** L29
[11] Szezech Jr J, Caldas I, Lopes S, Morrison P J and Viana R L 2012 *Phys. Rev. E* **86** 036206
[12] Budisica M and Thiffeault J L 2015 *Chaos* **25** 087407
[13] Haller G 2015 *Annual Review of Fluid Mechanics* **47** 137
[14] Haller G and Yuan G 2000 *Physica D: Nonlinear Phenomena* **147** 352
[15] Borgogno D, Grasso D, Pegoraro F and Schep T J 2011 *Physics of Plasmas* **18** 102307
[16] Rubino G, Borgogno D, Veranda M, Bonfiglio D, Cappello S and Grasso D 2015 *Plasma Phys. Control. Fusion* **57** 085004
[17] Di Giannatale G, Falessi M V, Grasso D, Pegoraro F and Schep T J 2018 *Physics of Plasmas* **25** 052306
[18] Di Giannatale G, Falessi M V, Grasso D, Pegoraro F and Schep T J 2018 *Physics of Plasmas* **25** 052307
[19] Falessi M V, Pegoraro F and Schep T J 2015 *Journal of Plasma Physics* **81** 05
[20] Haller G 2011 *Physica D: Nonlinear Phenomena* **240** 574
[21] Borgogno D, Grasso D, Porcelli F, Califano F, Pegoraro F and Farina D 2005 *Physics of Plasmas* **12** 032309
[22] Onu K, Huhn F and Haller G 2015 *Journal of Computational Science* **7** 26
[23] Cappello S and Biskamp D 1996 *Nuclear Fusion* **36** 571
[24] Veranda M et al. 2017 *Nuclear Fusion* **57** 116029
[25] Cappello S and Escande D F 2000 *Phys. Rev. Lett.* **85** 3838
[26] Escande D F et al. 2000 *Phys. Rev. Lett.* **85** 1662
[27] Escande D F, Paccagnella R, Cappello S, Marchetto C and D'Angelo F 2000 *Phys. Rev. Lett.* **85** 3169
[28] Piovesan P et al. 2009 *Nuclear Fusion* **49** 085036
[29] Gobbin M, Franz P, Auriemma F, Lorenzini R and Marrelli L 2015 *Plasma Phys. Control. Fusion* **57** 095004
[30] Cambon B, Leoncini X, Vittot M, Dumont R and Garbet X 2014 *Chaos* **24** 033101